Director orientation and optical stripe texture in electroclinic liquid crystals

F. J. Bartoli, J. R. Lindle, and S. R. Flom
Optical Sciences Division, Naval Research Laboratory, Washington, D.C. 20375-5338

R. Shashidhar, G. Rubin, J. V. Selinger, and B. R. Ratna
Center for Bio/Molecular Science and Engineering, Naval Research Laboratory, Washington, D.C. 20375-5348

(Received 16 June 1998)

We report the appearance of two types of optical stripes with different spatial wavelengths in electroclinic liquid crystals exhibiting a layer deformation. The periodicity of one set of stripes (longer wavelength) scales as twice the thickness of the cell, while the second (shorter wavelength) set of stripes has a periodicity that is independent of the thickness. Finally, detailed data on the spatially resolved optical studies of the stripe texture are presented which suggest the origin of the two types of stripe deformation and provide a possible explanation of their dependence on electric field. [S1063-651X(98)13211-7]

PACS number(s): 61.30.Eb

I. INTRODUCTION

Chiral smectic-*A* liquid crystals exhibit the electroclinic effect wherein the molecules tilt in the layer plane on application of the electric field [1]. In materials where the field-induced tilt angle is large, the layers buckle due to the strain accompanying the decrease in layer thickness [2,3]. The resulting modulation of the layer appears as a stripe texture when viewed in an optical microscope between crossed polarizers. Although initial studies indicated a triangular profile for the layer deformation [2], more detailed studies, coupled with an analysis based on continuum smectic free energy, showed a continuous evolution from sinusoidal to solitonlike profiles with increasing strength of the electric field [4]. Although it is to be expected that the optical stripes should have a detrimental effect on the contrast ratio, our initial results [5] indicated that the contrast ratio for a large beam size may be similar to that measured for a beam small compared to the stripe width. This result in turn indicates that the director orientation within each stripe itself is probably not uniform.

In this paper we report in more detail the results of our spatially resolved optical studies of the stripes which show that the molecular orientation within the stripes is nonuniform. In addition, we report the observation of a ''second set'' of optical stripes, which is of shorter wavelength than the stripes reported earlier. This observation is consistent with the recent results of Tang and Sprunt [6]. Finally, we also show that the wavelengths of the two sets of stripes have different dependencies on cell thickness, and discuss the possible origin of this stripe modulation pattern.

II. EXPERIMENT

A. Sample preparation and characterization

The liquid-crystal material studied is KN125 [2,7], whose phase behavior has been reported earlier. It exhibits a broad range of smectic-*A* phase (from 33 to 78 °C). Samples were prepared using commercial (EHC) cells treated for a planar alignment. The cell thickness was determined interferometrically prior to filling with the liquid crystal. A good planar alignment was obtained by cooling from the isotropic phase in the presence of an ac electric field. The field was removed in the smectic-*A* phase and the alignment was retained.

Absorption spectra taken using a Perkin-Elmer Lambda 9 spectrophotometer show that KN125 is transparent in the visible and near-ir spectral regions. The same instrument was used with polarization optics to determine the temperature and wavelength dependence of the birefringence. Experimental values of Δn obtained between 20 and 70 °C were fit using the expression $\Delta n = G(T)(1/\lambda_0^2 - 1/\lambda^2)^{-1}$, as discussed by Wu [8]. The best fit was obtained for $\lambda_0 = 0.2175\ \mu$m and $G(T) = 2.8780 - 0.0108\ \mathrm{T}\ \mu\mathrm{m}^{-2}$, where T is the temperature in degrees centigrade.

B. Polarization micrographs

For these studies the cell was placed between crossed polarizers in an optical microscope and photographs were taken under a bipolar electric field (10 Hz) with variable amplitude. The photographs were scanned into a computer and analyzed using Image-Pro Plus software.

C. Phase retardation measurements

Spatially resolved phase retardation experiments were performed using the focused output from a tunable cw argon ion (488.0–514.5 nm) or cw helium-neon (632.8 nm) laser. The wavelength was chosen for each sample thickness (and resulting phase angle δ) to provide a large change in transmission with field. The laser output was mechanically chopped at 12.5 Hz with a 5% duty cycle and field-dependent measurements were made by synchronizing bipolar square electrical pulses with the optical pulses. The chopped laser beam was expanded to fill the aperture of a Glan-Air polarizer, directed through a Babinet-Soliel compensator which was adjusted for half-wave retardation at the laser wavelength, and focused onto the liquid crystal sample using an $f/5$ lens system. The light transmitted through the sample is recollimated, directed through an analyzing Glan-Air polarizer, and detected by a photodiode. The measured extinction with the sample removed was $\approx 10^{-4}$.

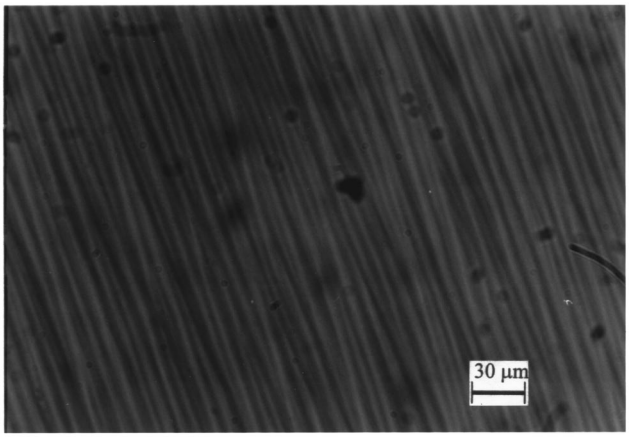

FIG. 1. Polarization micrographs of the stripe deformation in electroclinic liquid-crystal cells of 4 μm thickness.

For these studies, sample thicknesses were less than the Raleigh range of the $f/5$ focusing optics (approximately 20 μm at 632.8 nm) to assure reasonably planar wavefronts within the interaction volume. The $1/e$ beam radii at focus, measured by knife edge scans, were near-diffraction-limited at 2.0 and 2.75 μm for 488.0 and 632.8 nm radiation, respectively. For precise positional control, the liquid-crystal cell was mounted on an *xyz* translation stage equipped with differential micrometers on the *y* and *z* axes and with computer-controlled translation (1 μm resolution) of the *x* axis. The cell surface was aligned in the *x*-*z* plane and the field was applied in the *y* direction, the direction of light propagation. The homogeneously aligned samples were oriented so that the stripes, which are parallel to the unperturbed smectic layer normal, lie along the *z* axis. The polarized transmission was measured as the sample was scanned along the *x* axis, while the light polarization angle was kept constant.

III. RESULTS AND DISCUSSION

A. Observation and analysis of the second set of stripes

For an overview of the stripe deformity we studied polarization micrographs of cells of thickness 2, 4, 10, 15, and 25 μm under electric fields varying from 0 to 15 V/μm. Typical optical micrographs are shown in Figs. 1 and 2. All the cells show stripes with a periodic spatial modulation, the period of this modulation depending on the thickness. In the case of thicker cells, a second modulation of shorter wavelength is observed (see Fig. 2). The second set of stripes is inclined at an angle of about 15° to the larger-wavelength stripes.

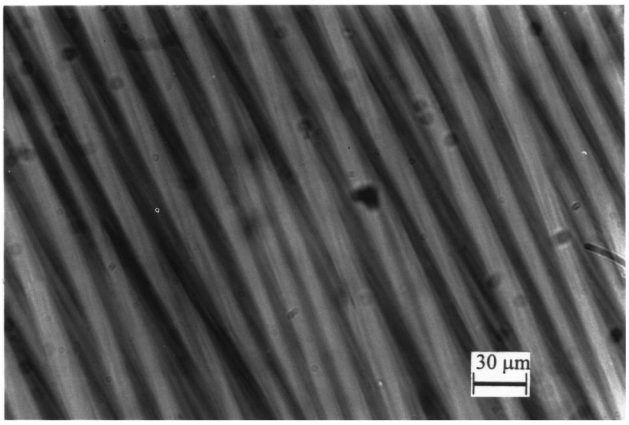

FIG. 2. Polarization micrograph of the stripe deformation for a 15-μm-thick cell.

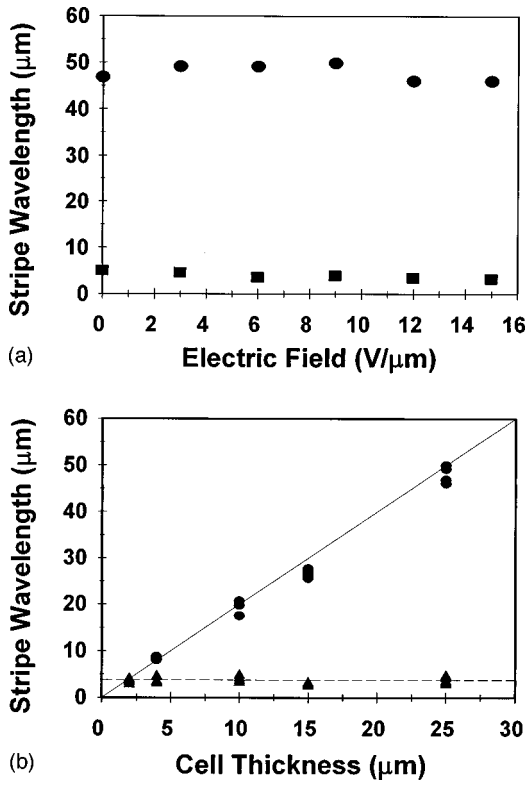

FIG. 3. (a) The measured stripe wavelength vs electric field for a 25 μm cell; (b) the measured stripe wavelength Λ vs cell thickness D. Data for all electric fields that were studied are shown together, because the wavelength is found to be independent of electric field. The solid line indicates the theoretical prediction $\Lambda = 2D$ for the longer-wavelength stripes; the dashed line indicates the constant value of $\Lambda = 3.8$ μm for the shorter-wavelength stripes.

To investigate the wavelengths of the two modulations, we first examined their dependence on electric field. We scanned the images, measured the intensity as a function of position, and determined the two periodicities as functions of electric field and cell thickness. Figure 3(a) shows the wavelength as a function of electric field for both modulations in a 25 μm cell. While there is some random scatter in the data, there is no systematic dependence on electric field. Similar results (not shown) were found for all the other cell thicknesses studied. Thus the strength of the electric field does not influence the wavelength of either modulation.

Figure 3(b) shows the data for the two wavelengths as functions of cell thickness combining the data for all values of the electric field. It is seen that the longer-wavelength modulation has a wavelength that depends linearly on cell thickness. This is similar to the thickness dependence of the stripe wavelength in ferroelectric liquid crystals found by Fünfschilling and Schadt [9]. By contrast, the shorter-wavelength modulation has a fixed wavelength of approximately 3.8 μm, which is independent of cell thickness as well as electric field. For 2μm cells, the two modulation wavelengths coincide; the extrapolation of the long-

wavelength modulation to a 2 μm cell gives a wavelength of about 4 μm, the same as the shorter-wavelength modulation.

The dependence of the longer-wavelength modulation on the cell thickness can be analyzed in terms of theoretical predictions for wavelength selection in this system. Shao *et al.* [10] have developed a model for wavelength selection in these electroclinic cells based on the past history of the modulation. They argue that the stripe modulation develops out of a chevron distortion across the thickness of the cell, and hence that the stripe width is equal to the cell thickness. Because the periodicity of the modulation is two stripes, this argument predicts that the wavelength is twice the cell thickness. Davey and Crossland [11] have developed a model for wavelength selection in ferroelectric liquid-crystal-based cells on electrohydrodynamics, which might also be applied to electroclinic liquid-crystal cells. They argue that the modulation develops out of convective rolls in the cells. Because these convective rolls are approximately circular, the stripe width is approximately equal to the cell thickness. Hence, although these two models are quite different, they both make the same prediction for wavelength selection: the wavelength should be twice the cell thickness, independent of material-dependent properties such as the elastic constants. By contrast, in any model based on minimization of an equilibrium free energy, one would expect the wavelength to depend on the elastic constants as well as the cell thickness. Thus, it is important to determine experimentally whether the wavelength is actually twice the cell thickness.

To answer that question, we superimpose the solid line with a slope of 2 on top of the experimental data in the stripe wavelength versus thickness plot of Fig. 3(b). This line agrees very well with the data for the longer-wavelength stripes over the whole range of cell thickness studied. It should be pointed out that this line represents a theoretical prediction with no adjustable parameters. The excellent agreement with experiment supports the concept that the wavelength is determined by the past history of the distortion or by electrohydrodynamics rather than by minimization of an equilibrium free energy.

The shorter-wavelength modulation has not been studied theoretically in any earlier work. As illustrated by the dashed line in Fig. 3(b), this modulation has a constant wavelength of 3.8 μm, independent of both electric field and cell thickness. The value of this wavelength is presumably determined by some material-dependent properties of the liquid crystal. Later in this paper, we will propose a model for this modulation based on the difference between the bulk and surface regions of the cell. In a forthcoming paper [12], an alternative model will also be proposed, based on a chiral instability of the smectic layer.

B. Spatially resolved measurements of the director orientation in larger-wavelength stripes

We shall now turn our attention to the director orientation within the optical stripes, as probed by our spatially resolved experiments. The orientation of the molecular director in each region is examined by scanning the tightly focused laser beam across the stripe pattern and measuring the cross-polarized transmission. The focused beam is then positioned within a stripe domain and the optical extinction measured by tuning the polarization angle to a transmission minimum. If the deformation were triangular, total extinction would be expected for light focused within a uniform stripe domain, whereas a large optical beam extending over many stripe domains should have degraded extinction due to the averaging over molecular director orientations. Any nonuniformity in the director orientation within the stripe should degrade the extinction for a focused beam as well.

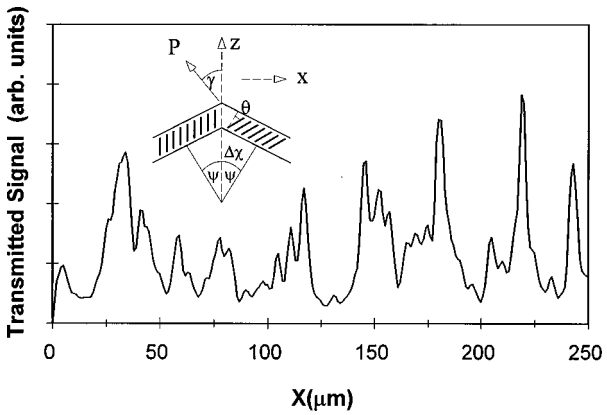

FIG. 4. x scan, transmitted signal as a function of x, for a 15-μm-thick KN125 sample placed between the crossed polarizers; the inset illustrates the experimental geometry (not to scale).

The intensity transmitted through a birefringent sample, interposed between crossed polarizers, is described by the expression [13]

$$I_{\perp} = I_0 \sin^2(\delta/2)\sin^2(2\phi), \tag{1}$$

where I_0 is the incident intensity, ϕ is the angle between the molecular director and the light polarization P, $\delta = 2\pi\Delta n d/\lambda$ is the phase angle, d is the sample thickness, λ is the wavelength, and Δn is the birefringence. The smectic layer deformation causes ϕ to vary spatially along the x direction. One can therefore write $\phi(x) = \gamma + \Psi(x) + \theta$, where γ denotes the angle between the polarization vector and the z axis, $\Psi(x)$ is the angle of the local layer normal relative to the z axis, and θ, the electroclinic tilt angle, is the angle between the local layer normal and the molecular director. Scanning the focused laser beam along x (perpendicular to the stripes) produces peaks and valleys in the cross-polarized transmission. These correspond to the light and dark stripes observed in the polarization micrographs of Figs. 1 and 2. This modulation reflects the spatial variation in the molecular director due to layer deformation. It can be seen from Eq. (1) that, while the magnitude of the transmitted signal depends on γ, θ, and δ, the amplitude of the modulation depends primarily on variations of $\Psi(x)$. For a triangular-wave layer deformation, $\Psi(x)$ should be constant within a given stripe, with its sign alternating between adjacent stripes.

Figures 4 and 5 show scans along the x direction (perpendicular to the stripes) for 15 and 4 μm cells, respectively. The inset in Fig. 4 illustrates the experimental geometry. The modulation seen in these figures is a direct indication of spatial variations in the layer normal. The square-wave spatial modulation of the transmission, expected for a simple triangular deformation, is not observed. This suggests that the distribution of molecular directors is not uniform within the stripes.

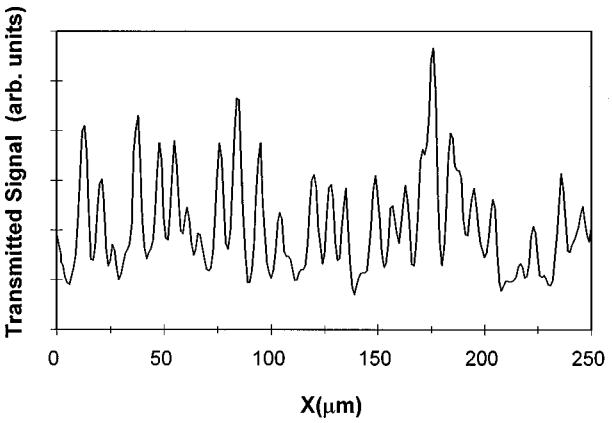

FIG. 5. x-scan data for a 4-μm-thick KN125 sample placed between crossed polarizers.

A nonuniform molecular alignment within the layers should also affect the extinction of the optical beam in the cross-polarized geometry. Evidence for this is shown in Fig. 6, which plots the field dependence of the transmission minimum ($I_{\min}$) for a 10-μm-thick cell, for both tightly focused (circles and squares) and unfocused (triangles) beams. In the figure, $I_{\min}$ is normalized to the transmission maximum ($I_{\max}$) in order to remove the phase dependence of $I_{\min}$ [see Eq. (1)]. No strong variation of $I_{\min}/I_{\max}$ with field is observed for this cell thickness. More importantly, the extinction measured for focused laser beams is close to that for an unfocused beam. The observed extinction for the focused beams is much poorer than predicted by the triangular model, indicating a nonuniform distribution of molecular directors within the stripes.

Equation (1) may be generalized to incorporate a position-dependent local layer normal. Assuming a large optical beam and, for simplicity, that ψ varies only with x, one obtains

$$I_{\perp} = I_0 \sin^2(\delta/2)(1/\Lambda)\int_0^{\Lambda} \sin^2[2\gamma + 2\psi(x) + 2\theta]dx, \tag{2}$$

where the transmitted intensity is averaged over Λ, the stripe period. For a symmetric triangular wave deformation, $\Psi(x)$ is equal to $\pm\psi_0$, where the sign alternates for adjacent stripes, and Eq. (2) becomes [2]

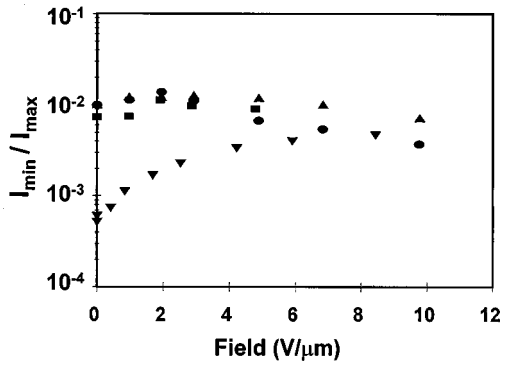

FIG. 6. The ratio $I_{\min}/I_{\max}$, as a function of electric field. Large-beam (▲) and focused-beam data (● and ■) for a 10-μm-thick sample are compared. Large-beam $I_{\min}/I_{\max}$ data for a 2-μm-thick sample (▼) is also shown for comparison.

$$I_{\perp} = 0.5 I_0 \sin^2(\delta/2)[\sin^2(2\gamma + 2\psi_0 + 2\theta) + \sin^2(2\gamma - 2\psi_0 + 2\theta)]. \tag{3}$$

The two terms within square brackets correspond to the transmission in adjacent stripe domains. It follows from Eq. (3) that the minimum occurs at $\gamma + \theta = 0$, whereas the maximum occurs at $\gamma + \theta = \pi/4$. Consequently, the extinction is related to the deformation angle by

$$\frac{I_{\min}}{I_{\max}} = \frac{\sin^2(2\psi)}{\sin^2(2\psi + \pi/2)} = \tan^2(\Delta\chi), \tag{4}$$

where $\Delta\chi = 2\psi_0$ is the full deformation angle.

One can estimate the $I_{\min}/I_{\max}$ expected for a triangular stripe profile by using the value $\Delta\chi = 15°$ measured by x-ray techniques [2]. Equation (4) then yields $I_{\min}/I_{\max} = 0.07$, which is nearly an order of magnitude larger than the experimental data in Fig. 6. This again suggests that the distribution of molecular directors within a stripe is nonuniform. Furthermore, it implies that use of the triangular deformation model to describe layer buckling would substantially underestimate achievable device contrast ratios.

To obtain a better description of the stripe deformation, we first note that the assumption of abrupt discontinuities at the stripe boundaries is unphysical. This can be avoided by considering a sinusoidal deformation, which is smoothly varying at the stripe boundary, but which otherwise closely approximates the triangular profile. The resulting variation of the molecular directors within a stripe should degrade the extinction of a tightly focused beam. Concurrently, the extinction obtained using a large beam should improve since the average value of ψ decreases. Assume a sinusoidal angular distribution of the form $\psi(x) = \psi_0 \sin(2\pi x/\Lambda_1)$, where $\psi_0 = 7.5°$ and Λ_1 defines the spatial period of the stripes. Equation (2) then predicts $I_{\min}/I_{\max} \approx 0.035$, in slightly better agreement with experiment. The origin of the remaining discrepancy is suggested by the appearance of the second shorter-wavelength modulation in the photomicrographs and x-scan data shown above. To approximate its effect on $I_{\min}/I_{\max}$, we simulate the double modulation using the simple angular distribution $\psi(x) = \psi_0 \sin(2\pi x/\Lambda_1)[\sin(2\pi x/\Lambda_2) + 1]/2$. Assuming $\Lambda_2 = \Lambda_1/4$ and $\psi_0 = 7.5°$, this distribution leads to even better agreement with experiment yielding $I_{\min}/I_{\max} = 0.013$. Although the precise nature of the short-wavelength modulation is not yet clear, these simulations indicate the significance of director variations within a stripe domain.

Some insight is obtained from Fig. 7, which shows the angular dependence of the normalized cross-polarized transmission for a large optical beam on a 2-μm-thick sample, where the applied field is varied up to 8.4 V/μm. These angular scans are plotted on a logarithmic scale to emphasize the minimum in optical transmission and the curves are fits to the data obtained using Eq. (2). The field-induced deformation progressively spoils extinction as the field increases. For the 2-μm-thick sample, this process appears to be entirely reversible and the transmission minimum returns to its initial value after the field is removed. This suggests that, unlike for the thicker samples, the deformation takes place within the elastic limit. The magnitude of $I_{\min}/I_{\max}$, plotted

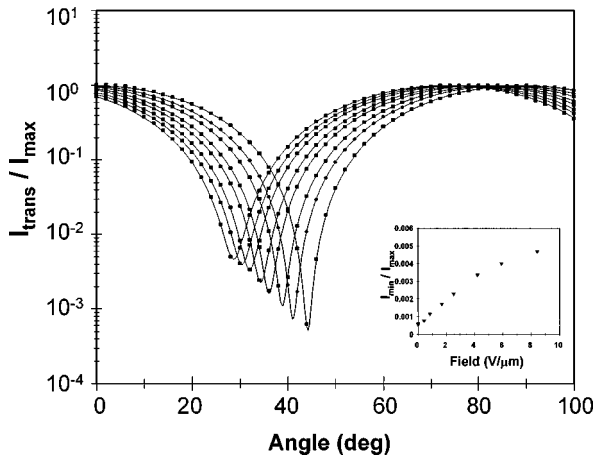

FIG. 7. Large beam $I_{\text{trans}}/I_{\max}$ vs polarization angle for a 2-μm-thick sample at various electric field strengths. The inset shows the field dependence of $I_{\min}/I_{\max}$.

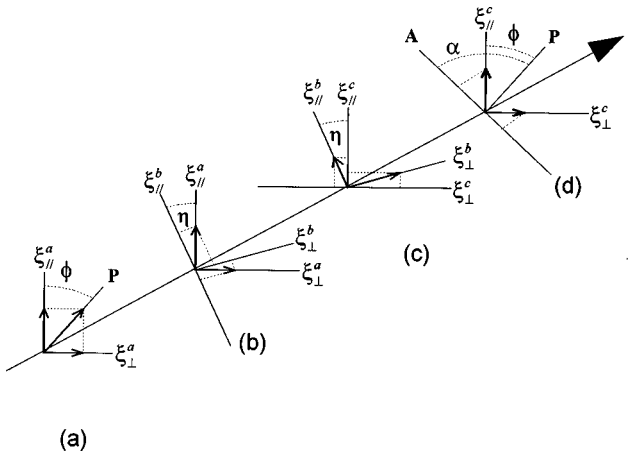

FIG. 8. Illustration of the propagation geometry for an optical field in a stratified three-layer birefringent medium.

in the inset in Fig. 7, increases monotonically with electric field. This field dependence is reminiscent of that of the electroclinic tilt angle, and is consistent with the picture of a distortion of the smectic layers due to the electroclinic deformation. For the 2 μm sample, $I_{\min}/I_{\max}$ is found to vary approximately as the square of the electroclinic tilt angle. These data are also plotted in Fig. 6 for comparison to the results for thicker cells. It is seen that at zero field $I_{\min}/I_{\max}$ is significantly lower than that observed for thicker samples, but is of comparable magnitude at large fields.

The above data suggest that the observed short-wavelength spatial modulation arises from the surface region, while the long-wavelength modulation, whose period varies with sample thickness, is characteristic of the bulk region. This is consistent with the fact that the short-wavelength modulation does not depend on sample thickness and that its field dependence is reversible, since greater restoring forces are expected to exist in the region near the surface. Polarization microscopy supports this picture since the short-wavelength modulation seems to disappear at 0 V, whereas the longer-wavelength variations do not. Moreover, it has been reported [14] that the electroclinic response time depends on the sample thickness suggesting that the surface and bulk respond differently and that surface interactions have a significant affect on the electro-optical response. A more general treatment of the angular distribution should account for such surface interactions.

A three-layer model, which treats the active region as a stratified birefringent material composed of a bulk layer sandwiched between surface regions, has been developed to quantitatively analyze the director orientation. This model is discussed in the next section.

C. Three-layer model

Figure 8 illustrates a three-layer model that treats the active region as a stratified birefringent material composed of a bulk layer sandwiched between two identical surface regions of thickness h_s. The bulk layer thickness is $h_b = D - 2h_s$, where D is the cell thickness.

The figure also shows the orientation of the optical axis within each layer relative to that of the polarizer (P) and analyzer (A), and illustrates the propagation of the optical beam through the stratified birefringent medium. The first three coordinate frames represent the alignment of the optical axis in the bulk layer and the surface layers, and are related by a rotation about the propagation axis y.

The analyzer orientation is indicated in the last coordinate frame. In the first surface region (a) the polarized electric field E_P is shown projected onto the principal axes denoted $\xi_{\parallel}^a$ and $\xi_{\perp}^a$. The field components $E_{\xi_{\parallel}^a} = E_P \cos\phi$ and $E_{\xi_{\perp}^a} = E_P \sin\phi$ have spatially modulated amplitudes through $\phi(x)$ and propagate through this region with different velocities, so that $E_{\xi_{\perp}^a}$ is retarded relative to $E_{\xi_{\parallel}^a}$. The emerging field is then incident on the bulk layer (b) whose major axis is rotated by an angle $\eta(x)$ relative to that of the first surface region. The projection of the field along the principal axes $\xi_{\parallel}^b$ and $\xi_{\perp}^b$ yields $E_{\xi_{\parallel}^b} = E_{\xi_{\parallel}^a}\cos\eta - E_{\xi_{\perp}^a}\sin\eta$ and $E_{\xi_{\perp}^b} = E_{\xi_{\perp}^a}\cos\eta + E_{\xi_{\parallel}^a}\sin\eta$, which vary with x in both amplitude and phase because of the modulation in $\phi(x)$ and $\eta(x)$. Again the slow component of the field is retarded as it propagates through the bulk layer. The second surface region (c) is assumed to be identical to the first ($\xi_{\parallel}^c = \xi_{\parallel}^a$ and $\xi_{\perp}^c = \xi_{\perp}^a$), giving $E_{\xi_{\parallel}^c} = E_{\xi_{\parallel}^b}\cos\eta + E_{\xi_{\perp}^b}\sin\eta$ and $E_{\xi_{\perp}^c} = E_{\xi_{\perp}^b}\cos\eta - E_{\xi_{\parallel}^b}\sin\eta$. The field components exiting the liquid crystal contain a comingling of the phases introduced by the individual layers. These are projected along the analyzer axis which is at an angle α relative to the polarizer, yielding $E_1 = E_{\xi_{\parallel}^c}\cos(\phi-\alpha)$ and $E_2 = E_{\xi_{\perp}^c}\sin(\phi-\alpha)$.

The light intensity transmitted by the analyzer for a particular x is given by

$$I = I_1 + I_2 + 2\sqrt{I_1 I_2}\,\cos\beta, \tag{5}$$

where the phase difference β and the square amplitudes I_j for the two waves, vary with x due to the stripe modulation in each region. To calculate the spatially modulated light transmission, Eq. (5) is evaluated as a function of x.

Figure 9 is a plot of the simulated x scan for cell thicknesses of 4, 8, and 16 μm. The front and rear surface regions were assumed to be 2 μm thick. For the 4-μm-thick sample ($h = 2$ μm; bulk thickness is equal to 0), the x scan is sinusoidal with a 4 μm period, similar to that observed experi-

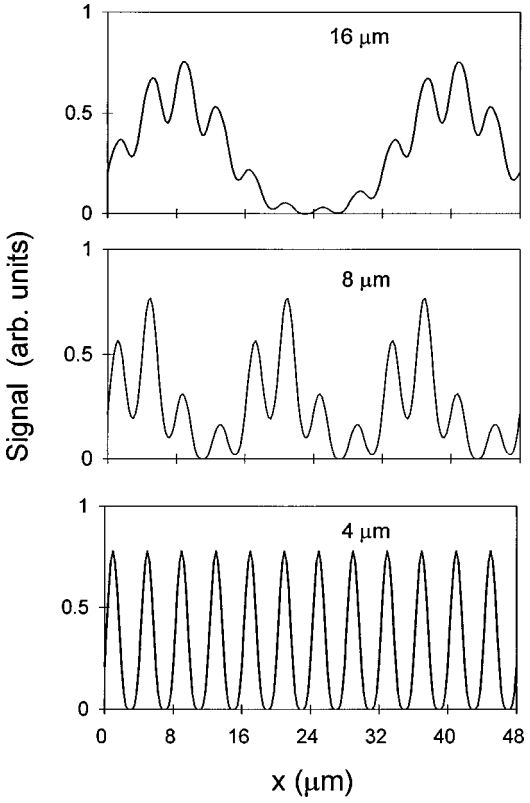

FIG. 9. Calculated transmission vs x for cell thicknesses of 4, 8, and 16 μm.

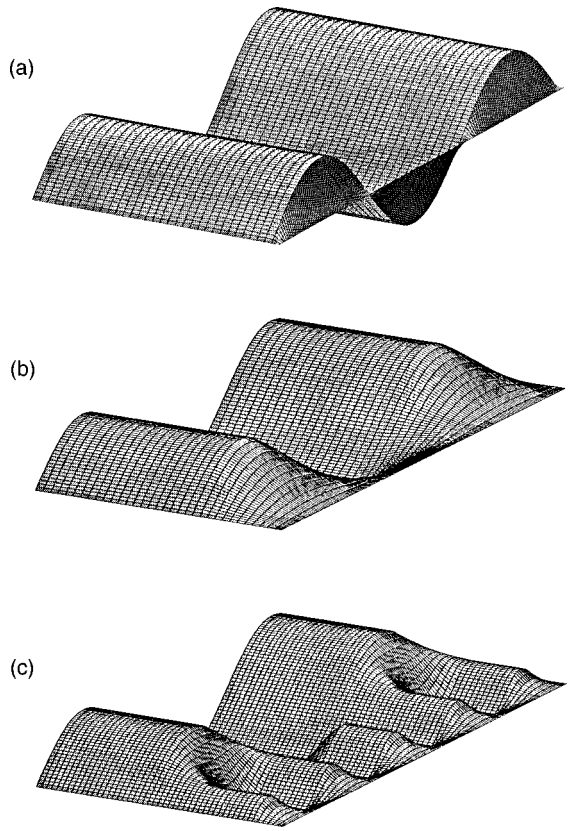

FIG. 10. Illustration of y-dependent stripe deformation.

mentally. The transmission for the 8 μm cell is more irregular and shows evidence for the long-wavelength modulation, whereas for the 16 μm cell a 32 μm period predominates with a short-wavelength modulation superimposed on it. This is reminiscent of the data in Figs. 4 and 5 and the photomicrographs of Figs. 1 and 2. The calculations provide qualitative agreement with the stripe patterns measured by phase retardation experiments and polarization microscopy.

The above discussion implies discontinuities in layer deformation at the boundaries between surface and bulk regions. These are clearly unphysical, and the stripe deformation probably involves smoothly varying variations in the local layer normals, as illustrated in Fig. 10. Figure 10(a) depicts a simple sinusoidal stripe geometry. This eliminates the unphysical discontinuities between stripes that are implied in the triangular model. However, this picture is not very satisfying because it implies enormous strains at the cell windows. For example, assuming a sinusoidal stripe with a 10 μm period and ψ_0 equal to 7.5°, the peak displacement in the smectic layer is found to be 0.2 μm. It is not reasonable that the stripe deformation end abruptly at the cell surface as illustrated in Fig. 10(a). Figure 10(b) illustrates a smoothly varying deformation between the constraining alignment layer and the liquid crystal. However, it still implies a single wavelength in the modulation pattern, which we know is contrary to the experimental results. Figure 10(c) depicts a smoothly varying deformation involving two modulation wavelengths, e.g., one surface region and the bulk region. It can be seen that those values of x for which both stripe modulations are in phase (or out of phase) could explain some of the sharp features observed in the x-scan data.

The period of the deformation in this bulk region is largely determined by the cell thickness. As discussed earlier, the extinction data in Fig. 6 suggest that the stripes associated with the bulk region involve an irreversible layer deformation that does not disappear when the field is removed. Such a permanent stripe texture has been observed previously in electroclinic liquid crystals [3]. The short wavelength shown for the region near the alignment surface of the cell is independent of the overall cell thickness. This reversible short-wavelength deformation appears to be associated with an elastic strain induced by the electroclinic tilt of the molecules within the smectic layers. This is not unreasonable since this surface region should be under the strong influence of the alignment surface of the cell. While these results are only illustrative, they do provide a possible explanation of the experimental results discussed above and indicate that the surface region can have properties very different from the bulk liquid crystal and can significantly affect the electro-optical properties of the material.

IV. CONCLUSIONS

Optical microscopy and spatially resolved phase-retardation measurements provide insight into the structure of the field-induced stripe texture previously observed in electroclinic liquid crystals. Clear evidence is found for a nonuniform molecular alignment within a stripe domain; in fact, the triangular deformation model substantially underestimates achievable contrast ratios by nearly an order of magnitude. An examination of the photomicrographs reveals the presence of two spatially periodic features in the stripe deformation; the wavelength of the larger periodic structure scales as twice the sample thickness while that of the finer

structure is thickness independent. Neither of these wavelengths is field dependent. Analysis of the spatially resolved phase-retardation data suggests that the short-wavelength modulation is characteristic of a surface-controlled region, while the previously reported larger stripes are more typical of the bulk liquid crystal. Optical extinction data further suggest that the layer deformation in the surface region is reversible and disappears when the field is removed, opposite to that of the bulk region. A three-layer (surface-bulk-surface) model is developed and is shown to adequately describe the observed stripe texture. These results provide insight into the smectic layer deformation, and permit more realistic predictions of the optical performance of devices based on the electroclinic effect.

ACKNOWLEDGMENT

The financial support of the Office of Naval Research is gratefully acknowledged.

[1] S. Garoff and R. B. Meyer, Phys. Rev. Lett. **38**, 848 (1977).
[2] G. P. Crawford, R. E. Geer, J. Naciri, R. Shashidhar, and B. R. Ratna, Appl. Phys. Lett. **65**, 2937 (1994).
[3] A. G. Rappaport, P. A. Williams, B. N. Thomas, N. A. Clark, M. B. Ros, and D. M. Walba, Appl. Phys. Lett. **67**, 17 (1995).
[4] R. E. Geer, S. J. Singer, J. V. Selinger, B. R. Ratna, and R. Shashidhar, Phys. Rev. E **57**, 3059 (1998).
[5] J. R. Lindle, S. R. Flom, F. J. Bartoli, A. T. Harter, R. E. Geer, B. R. Ratna, and R. Shashidhar, Proc. SPIE **2408**, 40 (1995); J. R. Lindle, F. J. Bartoli, S. R. Flom, A. T. Harter, B. R. Ratna, and R. Shashidhar, Appl. Phys. Lett. **70**, 1536 (1997).
[6] A. Tang and S. Sprunt, Phys. Rev. E **57**, 3050 (1998).
[7] G. P. Crawford, J. Naciri, R. Shashidhar, and B. R. Ratna, Jpn. J. Appl. Phys., Part 1 **35**, 2176 (1996).
[8] S. T. Wu, Phys. Rev. A **33**, 1270 (1986).
[9] J. Fünfschilling and M. Schadt, Jpn. J. Appl. Phys., Part 1 **30**, 741 (1991).
[10] R. F. Shao, P. C. Willis, and N. A. Clark, Ferroelectrics **121**, 127 (1991).
[11] A. B. Davey and W. A. Crossland, Mol. Cryst. Liq. Cryst. Sci. Technol., Sect. A **263**, 325 (1995).
[12] J. V. Selinger, B. R. Ratna, and R. Shashidhar (unpublished).
[13] M. Born and E. Wolf, *Principles of Optics*, 3rd ed. (Pergamon, New York, 1965), p. 696.
[14] J. A. M. M. van Haaren and G. L. J. A. Rikken, Phys. Rev. A **40**, 5476 (1989).